

Weakly nonlinear versus semi-linear models of the nonlinear evolution of the centrifugal instability

Eunok Yim¹, Paul Billant^{2,†} and François Gallaire¹

¹LFMI, École Polytechnique Fédérale de Lausanne (EPFL), 1015 Lausanne, Switzerland

²Laboratoire d'Hydrodynamique (LadHyX), CNRS, Ecole Polytechnique, Institut Polytechnique de Paris, 91120 Palaiseau, France

(Received 27 May 2022; revised 1 November 2022; accepted 7 January 2023)

We carry out a weakly nonlinear analysis of the centrifugal instability for a columnar vortex in a rotating fluid, and compare the results to those of the semi-linear model derived empirically by Yim *et al.* (*J. Fluid Mech.*, vol. 897, 2020, A34). The asymptotic analysis assumes that the Reynolds number is close to the instability threshold so that the perturbation is only marginally unstable. This leads to two coupled equations that govern the evolutions of the amplitude of the perturbation and of the mean flow under the effect of the Reynolds stresses due to the perturbation. These equations differ from the Stuart–Landau amplitude equation or coupled amplitude equations involving a mean field that have been derived previously. In particular, the amplitude does not saturate to a constant as in the supercritical Stuart–Landau equation, but decays afterwards reflecting the instability disappearance when the mean flow tends toward a neutrally stable profile in the direct numerical simulations (DNS). These equations resemble those of the semi-linear model except that the perturbation in the weakly nonlinear model keeps at leading order the structure of the eigenmode of the unperturbed base flow. The predictions of the weakly nonlinear equations are compared to those of the semi-linear model and to DNS for the Rossby number $Ro = -4$ and various Reynolds numbers and wavenumbers. They are in good agreement with the DNS when the growth rate is sufficiently small. However, the agreement deteriorates and becomes only qualitative for parameters away from the marginal values, whereas the semi-linear model continues to be in better agreement with the DNS.

Key words: instability, vortex flows, nonlinear dynamical systems

† Email address for correspondence: billant@ladhyx.polytechnique.fr

1. Introduction

Simplified models in hydrodynamics are generally useful to understand the underlying physics or to obtain first results without the large computational cost of direct numerical simulations (DNS). To derive such models, two methods are generally available: either deriving a rigorous model by asymptotic analyses when one parameter is small, or obtaining an empirical model based on heuristic assumptions (Manti-Lugo, Arratia & Gallaire 2014; Meliga 2017).

By adopting the second approach, recently Yim, Billant & Gallaire (2020) have proposed a semi-linear model of the nonlinear evolution of a spatially periodic instability. The idea consists in taking into account only the dynamics of the most unstable perturbation and the spatially averaged mean flow, whereas higher harmonics are neglected. Hence the semi-linear model is made of two coupled equations governing the evolution of the most unstable perturbation on the spatially averaged mean flow and the mean flow under the effect of the spatially averaged Reynolds stresses due to the perturbation. The only difference compared to pure linear equations is the evolution of the mean flow.

Such a semi-linear model turns out to be similar to the early method proposed by Stuart (1958) to describe the saturation of supercritical spatially periodic instabilities. A difference, however, is that Stuart (1958) has neglected the time derivative in the mean-flow equation by arguing that it should be negligible at large times. He has then obtained an approximate Stuart–Landau amplitude equation from the integral equation of energy balance for the disturbance by assuming that the latter remains identical in shape to the fundamental eigenmode given by the unperturbed base flow. Later, rigorous weakly nonlinear derivations for the supercritical instabilities observed in the plane Poiseuille or Taylor–Couette flows (Stuart 1960; Watson 1960; Davey 1962) have shown that the generation of harmonics and distortion of the fundamental mode should be taken into account in these cases.

Although general, the semi-linear model has been developed by Yim *et al.* (2020) in the specific case of the centrifugal instability of a columnar vortex in a rotating fluid. A very good agreement between the semi-linear model and DNS has been found for the Rossby number $Ro = -4$ and up to the highest Reynolds number investigated, namely $Re = 2000$. The results show that the nonlinear evolution of the centrifugal instability redistributes the mean absolute angular momentum towards a profile that is stable according to the Rayleigh criterion (Kloosterziel, Carnevale & Orlandi 2007; Carnevale *et al.* 2011; Yim *et al.* 2020). Subsequently, the perturbations decay, i.e. the centrifugal instability ceases.

Here, we derive rigorously weakly nonlinear equations for the same instability, and we compare their predictions to those of the empirical semi-linear model as well as to DNS. The asymptotic analysis assumes that the Reynolds number is close to the critical value for instability so that the perturbations are only marginally unstable.

The paper is organized as follows. The problem is formulated in § 2. The governing equations are given in § 2.1 and then rewritten in a convenient form in § 2.2. The linear stability of the flow is recalled in § 2.3. The weakly nonlinear analysis is conducted in § 3. The semi-linear model is summarized briefly in § 4, and the numerical methods are described in § 5. The results of the weakly nonlinear model, semi-linear model and DNS are mutually compared in § 6, before conclusions are drawn in § 7.

2. Problem formulation

2.1. Governing equations

As in Yim *et al.* (2020), we consider an axisymmetric vortex with initial non-dimensional velocity $\mathbf{u}_0 = (u_0, v_0, w_0) = (0, r \exp(-r^2), 0)$ in cylindrical coordinates (r, θ, z) . The time and length have been chosen so that the vortex radius and the maximum angular velocity are unity. The fluid is incompressible and rotating about the z axis:

$$\frac{\partial \mathbf{u}}{\partial t} + \mathbf{u} \cdot \nabla \mathbf{u} + 2Ro^{-1} \mathbf{e}_z \times \mathbf{u} = -\rho^{-1} \nabla p + Re^{-1} \nabla^2 \mathbf{u}, \quad (2.1)$$

$$\nabla \cdot \mathbf{u} = 0, \quad (2.2)$$

where \mathbf{e}_z is the unit vector in the z direction, p is the pressure, ρ is the constant density, $Ro = 2\Omega_c/f$ is the Rossby number, and $Re = \Omega_c R_0^2/\nu$ is the Reynolds number, with f the Coriolis parameter, Ω_c and R_0 the dimensional maximum angular velocity and radius of the vortex, and ν the viscosity.

Yim *et al.* (2020) studied the particular value $Ro = -4$ for several Reynolds numbers and showed that the dynamics remains always purely axisymmetric. For this reason, axisymmetry will be assumed here from the outset. The boundary conditions are therefore $u = v = 0$ at $r = 0$, and $\mathbf{u} \rightarrow 0$ as $r \rightarrow \infty$ (Batchelor & Gill 1962). The Rossby number will be also set to $Ro = -4$ throughout the paper, as in Yim *et al.* (2020).

2.2. Mean and fluctuation equations

Following Stuart (1958), Davey (1962) and Yim *et al.* (2020), it is first convenient to decompose the velocity and pressure as

$$[\mathbf{u}, p](r, z, t) = [\bar{\mathbf{U}}, \bar{P}](r, t) + [\hat{\mathbf{u}}, \hat{p}](r, z, t), \quad (2.3)$$

where $\bar{\mathbf{U}} = z_{max}^{-1} \int_0^{z_{max}} \mathbf{u} \, dz$ and $\bar{P} = z_{max}^{-1} \int_0^{z_{max}} p \, dz$ are the axially averaged mean quantities over the domain height z_{max} . Averaging (2.1)–(2.2) in z shows that the mean flow is purely azimuthal, $\bar{\mathbf{U}} = \bar{V}(r, t) \mathbf{e}_\theta$, and governed by

$$-\frac{\bar{V}^2}{r} - \frac{2}{Ro} \bar{V} = -\rho^{-1} \frac{\partial \bar{P}}{\partial r} - \overline{\mathcal{N}(\hat{\mathbf{u}}, \hat{\mathbf{u}})} \cdot \mathbf{e}_r, \quad (2.4)$$

$$\frac{\partial \bar{V}}{\partial t} = \frac{1}{Re} D^2 \bar{V} - \overline{\mathcal{N}(\hat{\mathbf{u}}, \hat{\mathbf{u}})} \cdot \mathbf{e}_\theta, \quad (2.5)$$

where

$$D^2 \cdot = \frac{\partial}{\partial r} \left(\frac{1}{r} \frac{\partial}{\partial r} (r \cdot) \right), \quad (2.6)$$

$$\mathcal{N}(\mathbf{a}, \mathbf{b}) = \mathbf{a} \cdot \nabla \mathbf{b} = \begin{pmatrix} a_r \frac{\partial b_r}{\partial r} + a_z \frac{\partial b_r}{\partial z} - \frac{a_\theta b_\theta}{r} \\ a_r \frac{\partial b_\theta}{\partial r} + a_z \frac{\partial b_\theta}{\partial z} + \frac{a_\theta b_r}{r} \\ a_r \frac{\partial b_z}{\partial r} + a_z \frac{\partial b_z}{\partial z} \end{pmatrix}. \quad (2.7)$$

It is convenient to further decompose the mean flow as

$$\bar{V}(r, t) = v_0(r) + \bar{v}(r, t), \quad (2.8)$$

where v_0 is the initial flow, so that (2.5) becomes

$$\frac{\partial \bar{v}}{\partial t} = \frac{1}{Re} D^2(\bar{v} + v_0) - \overline{\mathcal{N}(\hat{u}, \hat{u})} \cdot \mathbf{e}_\theta. \tag{2.9}$$

Subtracting (2.4) and (2.9) from (2.1) yields the equation for the perturbation \hat{u} :

$$\frac{\partial \hat{u}}{\partial t} + \mathcal{L}(\hat{u}) = -\mathcal{N}(\bar{u}, \hat{u}) - \mathcal{N}(\hat{u}, \bar{u}) - \mathcal{N}(\hat{u}, \hat{u}) + \overline{\mathcal{N}(\hat{u}, \hat{u})}, \tag{2.10}$$

$$\nabla \cdot \hat{u} = 0, \tag{2.11}$$

where $\bar{u} = \bar{v} \mathbf{e}_\theta$ and

$$\mathcal{L}(\hat{u}) = -2\Omega_0 \hat{v} \mathbf{e}_r + \zeta_0 \hat{u} \mathbf{e}_\theta + 2Ro^{-1} \mathbf{e}_z \times \hat{u} + \rho^{-1} \nabla \hat{p} - Re^{-1} \nabla^2 \hat{u}, \tag{2.12}$$

with $\Omega_0 = v_0/r$ and $\zeta_0 = 2\Omega_0 + r\Omega_0'$. We emphasize that (2.9)–(2.11) are only a convenient rewriting of (2.1)–(2.2), and no approximation has been done so far. In the absence of perturbation $\hat{u} = 0$, the total mean flow \bar{V} is governed by the diffusion equation (2.5) and there is a cyclostrophic balance along the radial direction (2.4).

2.3. Linear stability

When (2.10)–(2.11) are linearized and the viscous diffusion of the base flow is neglected so that $\bar{v} = 0$, they reduce to the stability problem

$$\frac{\partial \hat{u}}{\partial t} = -\mathcal{L}(\hat{u}), \tag{2.13}$$

$$\nabla \cdot \hat{u} = 0. \tag{2.14}$$

Here, we will consider the weakly nonlinear evolution of the most unstable perturbation of (2.13) for a given axial wavenumber k :

$$[\hat{u}, \hat{p}] = [\tilde{u}, \tilde{p}](r) \exp(\sigma t + ikz) + c.c., \tag{2.15}$$

where σ is the growth rate and *c.c.* denotes the complex conjugate.

When the Rossby number is in the range $Ro < -1$ or $Ro > \exp(2)$, a vortex with Gaussian angular velocity is unstable in the inviscid limit to the centrifugal instability according to the Rayleigh criterion, i.e. there exists some radius where $\phi < 0$, with $\phi = 2(\Omega_0 + 1/Ro)(\zeta_0 + 2/Ro)$ the Rayleigh discriminant. The inviscid growth rate is given by $\sigma_i = \sqrt{-\phi(r_0)}$, where r_0 is the radius where ϕ is minimum (Smyth & McWilliams 1998; Billant & Gallaire 2005) ($r_0 = 0.93$ and $\sigma_i = 0.3635$ for $Ro = -4$) and is reached in the limit of infinite axial wavenumber. When the Reynolds number is finite, the maximum growth rate and the most amplified wavenumber k_m decrease as the Reynolds number is reduced, as illustrated in figure 1(a) for $Ro = -4$. The instability is totally stabilized when $Re \sim 100$. Since viscous effects scale like k^2/Re at leading order for large axial wavenumber, they become active for wavenumbers typically such that $k^2 = O(Re)$.

Figure 1(b) displays the eigenmodes for $Re = 2000$ for two wavenumbers: $k = 8.6$ and $k = 23$. As in Yim *et al.* (2020), the eigenmode is normalized so that the maximum absolute vertical velocity is unity: $\max(|\tilde{w}|) = 1$. It can be seen that the eigenmode tends to be more localized as k increases and the amplitudes of the horizontal velocity components increase with k .

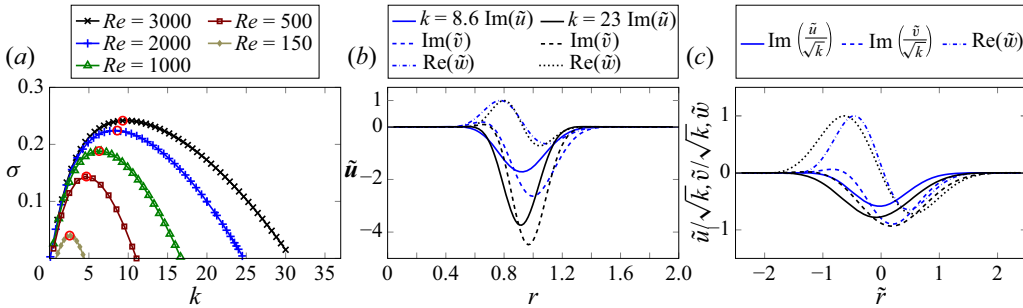


Figure 1. (a) Linear growth rate σ as a function of the axial wavenumber k for $Ro = -4$ and different Reynolds numbers: $Re = 150, 500, 1000, 2000$ and 3000 . The red circles indicate the maximum growth rate and corresponding most amplified axial wavenumber k . (b) Velocity components ($\tilde{u}, \tilde{v}, \tilde{w}$) of the eigenmodes as functions of r for $k = 8.6$ (blue lines) and $k = 23$ (black lines), for $Re = 2000$ and $Ro = -4$. (c) Same as (b), but the velocity components are rescaled as $(\tilde{u}/\sqrt{k}, \tilde{v}/\sqrt{k}, \tilde{w})$ and plotted as functions of $\tilde{r} = (r - r_0)\sqrt{k}$.

3. Weakly nonlinear analysis

3.1. Formulation

The first task in order to carry out a weakly nonlinear analysis is to identify some conditions under which the instability is only marginally unstable. There are several possible configurations: first, the Rossby number can be considered close to the critical Rossby numbers $Ro_c = -1$ or $Ro'_c = \exp(2)$; second, Ro can be considered arbitrary but Re close to the critical Reynolds number Re_c (figure 1); or, third, Ro and Re can be considered arbitrary but the axial wavenumber k can be assumed to be close to the viscous cut-off k_c where the growth rate vanishes (figure 1). Since the Rossby number $Ro = -4$ investigated in Yim *et al.* (2020) is relatively far from $Ro_c = -1$, we will consider herein the second configuration, i.e. the Reynolds number Re is assumed to be close to Re_c so that the eigenmode at the most unstable wavenumber k for this Reynolds number Re is marginally unstable. However, we will see later that the following analysis will also apply to the third configuration, i.e. near the viscous wavenumber cut-off. Accordingly, the order of magnitude of the growth rate can be used as a small parameter, i.e.

$$\sigma = \epsilon \tilde{\sigma}, \tag{3.1}$$

where $\tilde{\sigma} = O(1)$ and $\epsilon \ll 1$. Even if the Reynolds number is close to Re_c , we will consider that it is large such that

$$\frac{1}{Re} = \frac{\epsilon^2}{\tilde{Re}}, \tag{3.2}$$

with $\tilde{Re} = O(1)$. This distinguished limit will enable us to take into account the viscous diffusion at leading order. Nevertheless, the following analysis should remain valid if $1/Re \lesssim O(\epsilon^2)$, i.e if the Reynolds number is larger than imposed by (3.2), but not in the opposite case, $1/Re \gg O(\epsilon^2)$. Hence the scaling assumptions (3.1) and (3.2) can be combined into the condition $1/\sqrt{Re} \lesssim \sigma \ll 1$, meaning that the growth of the perturbation has to be slow but not too slow compared to the viscous diffusion. A paradoxical implication is that as the Reynolds number decreases (figure 1a), our approach will no longer be valid below a certain Reynolds number even if the growth rate is small, because the condition $1/\sqrt{Re} \lesssim \sigma$ will no longer be fulfilled. For the same reason, if the Rossby number is increased from below towards the critical value $Ro_c = -1$ for a fixed large

Reynolds number, the present analysis will cease to be valid when σ is typically smaller than $1/\sqrt{Re}$. In summary, we expect the scaling hypotheses (3.1) and (3.2) to be met only in an intermediate range of growth rate for given Reynolds and Rossby numbers. This will be confirmed in § 6 when the predictions of the weakly nonlinear analysis will be compared to DNS.

The scaling (3.2) together with the assumption of being close to the viscous threshold, i.e. $\sigma \simeq \sigma_i - k^2/Re \ll 1$, implies that $k^2/Re = O(1)$ since the maximum growth rate in the inviscid limit σ_i is of order unity for $Ro = -4$. In this way, viscous effects act on the perturbation despite the large Reynolds number limit considered in (3.2). This implies that the wavenumber is large:

$$k = \frac{\tilde{k}}{\epsilon}, \tag{3.3}$$

where $\tilde{k} = O(1)$. An unstable eigenmode is always accompanied by a stable counterpart with opposite growth rate in the inviscid limit due to time reversibility. Hence if the unstable eigenmode is marginally unstable, then the stable counterpart is also marginally stable and it needs to be taken into account in a weakly nonlinear analysis. However, (3.2) and (3.3) imply that such a stable mode is here strongly damped and does not need to be considered since its growth rate is $\sigma \simeq -\sigma_i - k^2/Re$, which is typically $O(1)$ and negative. For that reason, the resulting amplitude equations will be first order in time and dissipative, while similar inviscid instabilities in nature, such as the baroclinic instability or the Kelvin–Helmholtz instability, have been described by amplitude equations that are second order in time and thus reversible (Drazin 1970; Pedlosky 1970; Gibbon & McGuinness 1981).

In turn, the fact that the wavenumber is large implies that the eigenmode $[\tilde{u}, \tilde{p}](r)$ is strongly localized in a region of width $O(k^{-1/2}) = O(\epsilon^{1/2})$ around a particular radius r_0 , as shown by Bayly (1988). Hence the radial derivative is large,

$$\frac{\partial}{\partial r} = O(k^{1/2}), \tag{3.4}$$

meaning that each term of (2.10) needs first to be appropriately scaled before performing a weakly nonlinear analysis. We emphasize that the scaling (3.4) applies only to the perturbation \hat{u} and not to the initial mean flow v_0 . Since the eigenmode is normalized such that $\max(|\tilde{w}|) = 1$, the different velocity components and pressure of the disturbance then scale as (Bayly 1988)

$$\hat{u} = O(k^{1/2}), \quad \hat{v} = O(k^{1/2}), \quad \hat{w} = O(1), \quad \hat{p} = O(k^{-1}). \tag{3.5a-d}$$

Again, we stress that this scaling does not apply to the mean flow \bar{v} . In order to illustrate this scaling, the eigenmodes for $k = 8.6$ and $k = 23$ are rescaled according to (3.5a-d) and plotted as functions of $(r - r_0)\sqrt{k}$ in figure 1(c). The velocity components for the two wavenumbers collapse, although this is only approximate since k is not so large.

We will use the scaling (3.5a-d) only to obtain the leading-order magnitude of each operator in (2.10) since the linear problem will be solved numerically and not analytically as done by Bayly (1988). Using (3.4) and (3.5a-d), we have

$$\mathcal{L} = O(1), \quad \mathcal{N} = O(k), \quad D^2 = O(k), \quad \nabla = O(k). \tag{3.6a-d}$$

Hence we define the following rescaled variable and operators:

$$\tilde{r} = \frac{r - r_0}{\epsilon^{1/2}}, \quad \tilde{\mathcal{N}} = \epsilon \mathcal{N}, \quad \tilde{D}^2 = \epsilon D^2, \quad \tilde{\nabla} = \epsilon \nabla, \tag{3.7a-d}$$

where the operators with a tilde are of order unity at leading order. These operators could be split into different orders, e.g. $\tilde{\mathcal{N}} = \tilde{\mathcal{N}}_0 + \epsilon^{1/2}\tilde{\mathcal{N}}_1 + \dots$. However, this will not be done, to avoid long algebra. In addition, this is not necessary because the problem will be solved numerically as mentioned already.

Then the governing equations for the perturbation become

$$\frac{\partial \hat{\mathbf{u}}}{\partial t} = -\mathcal{L}(\hat{\mathbf{u}}) - \epsilon^{-1} \tilde{\mathcal{N}}(\bar{\mathbf{u}}, \hat{\mathbf{u}}) - \epsilon^{-1} \tilde{\mathcal{N}}(\hat{\mathbf{u}}, \bar{\mathbf{u}}) - \epsilon^{-1} \tilde{\mathcal{N}}(\hat{\mathbf{u}}, \hat{\mathbf{u}}) + \epsilon^{-1} \overline{\tilde{\mathcal{N}}(\hat{\mathbf{u}}, \hat{\mathbf{u}})}, \quad (3.8)$$

$$\tilde{\nabla} \cdot \hat{\mathbf{u}} = 0, \quad (3.9)$$

The important feature in (3.8) is that the nonlinear terms scale at leading order as $1/\epsilon$ because the axial wavenumber is large. Similarly, the equation for the mean flow (2.9) becomes

$$\frac{\partial \bar{\mathbf{v}}}{\partial t} = \frac{\epsilon}{\tilde{Re}} \tilde{D}^2 \bar{\mathbf{v}} + \frac{\epsilon^2}{\tilde{Re}} D^2 v_0 - \epsilon^{-1} \overline{\tilde{\mathcal{N}}(\hat{\mathbf{u}}, \hat{\mathbf{u}})} \cdot \mathbf{e}_\theta. \quad (3.10)$$

We can remark that the viscous diffusion of the mean flows $\bar{\mathbf{v}}$ and v_0 are not of the same order because the former varies over \tilde{r} according to (3.4), in contrast to the latter, which varies over r .

Nevertheless, (3.8)–(3.10) can be rewritten in a form close to the original (2.9)–(2.11) by simply rescaling the variables as $\bar{\mathbf{v}} = \epsilon \bar{\mathbf{v}}'$ and $[\hat{\mathbf{u}}, \hat{p}] = \epsilon [\hat{\mathbf{u}}', \hat{p}']$. This leads to

$$\frac{\partial \hat{\mathbf{u}}'}{\partial t} = -\mathcal{L}(\hat{\mathbf{u}}') - \tilde{\mathcal{N}}(\bar{\mathbf{u}}', \hat{\mathbf{u}}') - \tilde{\mathcal{N}}(\hat{\mathbf{u}}', \bar{\mathbf{u}}') - \tilde{\mathcal{N}}(\hat{\mathbf{u}}', \hat{\mathbf{u}}') + \overline{\tilde{\mathcal{N}}(\hat{\mathbf{u}}', \hat{\mathbf{u}}')}, \quad (3.11)$$

$$\tilde{\nabla} \cdot \hat{\mathbf{u}}' = 0, \quad (3.12)$$

$$\frac{\partial \bar{\mathbf{v}}'}{\partial t} = \frac{\epsilon}{\tilde{Re}} \tilde{D}^2 \bar{\mathbf{v}}' + \frac{\epsilon}{\tilde{Re}} D^2 v_0 - \overline{\tilde{\mathcal{N}}(\hat{\mathbf{u}}', \hat{\mathbf{u}}')} \cdot \mathbf{e}_\theta. \quad (3.13)$$

The governing equations are now in a suitable form to carry out the weakly nonlinear analysis. To do so, we expand the time, the mean flow and the perturbation as follows:

$$\frac{\partial}{\partial t} = \frac{\partial}{\partial t_0} + \epsilon \frac{\partial}{\partial t_1} + \epsilon^2 \frac{\partial}{\partial t_2} + \dots, \quad (3.14)$$

$$\bar{\mathbf{v}}' = \epsilon \bar{\mathbf{v}}_1 + \epsilon^2 \bar{\mathbf{v}}_2 + \dots, \quad (3.15)$$

$$[\hat{\mathbf{u}}', \hat{p}'] = \epsilon [\hat{\mathbf{u}}_1, \hat{p}_1] + \epsilon^2 [\hat{\mathbf{u}}_2, \hat{p}_2] + \dots. \quad (3.16)$$

In the following, the first-order mean flow will be further decomposed into two parts:

$$\bar{\mathbf{v}}_1 = \bar{\mathbf{v}}_{11}(\tilde{r}, t_1) + \bar{\mathbf{v}}_{10}(r, t_0), \quad (3.17)$$

where $\bar{\mathbf{v}}_{10}$ will vary over r due to the viscous diffusion of the base flow, whereas $\bar{\mathbf{v}}_{11}$ will vary over \tilde{r} due to its own viscous diffusion and the Reynolds stresses due to the perturbation.

Finally, we stress that we will consider a single axial wavenumber, i.e. no spatial modulation will be taken into account in the present analysis. The DNS performed by Yim *et al.* (2020) for $Ro = -4$ and $Re = 2000$ initialized by the eigenmode of the most amplified wavenumber has indeed demonstrated the absence of spatial modulation. This will be shown again for $Re = 500$ in § 6.

3.2. Order ϵ

At order ϵ , (3.11)–(3.13) reduce to

$$\frac{\partial \hat{\mathbf{u}}_1}{\partial t_0} = -\mathcal{L}(\hat{\mathbf{u}}_1), \tag{3.18}$$

$$\tilde{\nabla} \cdot \hat{\mathbf{u}}_1 = 0, \tag{3.19}$$

$$\frac{\partial \bar{v}_{10}}{\partial t_0} = \frac{1}{\tilde{Re}} D^2 v_0. \tag{3.20}$$

The solution of (3.18)–(3.19) is taken as the most unstable eigenmode:

$$\hat{\mathbf{u}}_1 = \tilde{\mathbf{u}}_1(\tilde{r}) \exp(ikz + \sigma t_0) + c.c.. \tag{3.21}$$

However, since the growth rate is assumed to be small, $\sigma = \epsilon \tilde{\sigma}$, we can rewrite (3.21) as

$$\hat{\mathbf{u}}_1 = A(t_1) \tilde{\mathbf{u}}_1(\tilde{r}) \exp(ikz) + c.c., \tag{3.22}$$

where A is an amplitude varying over the slow time t_1 . By defining the shift-operator (Meliga, Chomaz & Sipp 2009)

$$\tilde{\mathcal{L}} = \mathcal{L} - \epsilon \tilde{\sigma}, \tag{3.23}$$

we can approximate \mathcal{L} in (3.18) by $\tilde{\mathcal{L}}$, while the complementary $O(\epsilon)$ term will appear only at next order. In other words, (3.18) becomes

$$\frac{\partial \hat{\mathbf{u}}_1}{\partial t_0} = -\tilde{\mathcal{L}}(\hat{\mathbf{u}}_1) + O(\epsilon) = 0. \tag{3.24}$$

Hence the eigenvalues of the operator $\tilde{\mathcal{L}}$ correspond to those of \mathcal{L} shifted by $\epsilon \tilde{\sigma}$, whereas the eigenmodes remain identical.

Instead of using the shift-operator $\tilde{\mathcal{L}}$, one could alternatively expand the operator \mathcal{L} around the critical Reynolds number $Re_c(k)$ for a given wavenumber k , i.e. $\mathcal{L}(Re) = \mathcal{L}(Re_c) + (Re - Re_c) \partial \mathcal{L} / \partial Re + \dots$, and assume $Re - Re_c = O(\epsilon)$. Then, the truly marginally stable operator $\mathcal{L}(Re_c)$ would arise at leading order. The predictions of the amplitude equations derived by these two different methods have been compared by Gallaire *et al.* (2016) in the case of the supercritical Hopf bifurcation in the cylinder wake. They agree in the weakly nonlinear regime, but differ when the control parameter is far from threshold. Here, we have preferred the shift-operator method because it does not require us to compute additional operators such as $\partial \mathcal{L} / \partial Re$. In addition, the choice of a particular marginally unstable point is implicit and virtual when using a shift-operator since, in practice, it does not appear explicitly in the calculations. Therefore, the same weakly nonlinear analysis applies by considering another neutral point as long as the characteristics of the eigenvalue spectrum and the magnitudes of the parameters are similar. In particular, we will see that the resulting amplitude equations are also valid when the wavenumber k is close to the viscous cut-off k_c but Re is far from Re_c .

Finally, the solution of (3.20) is simply $\bar{v}_{10} = 4(r^2 - 2)r \exp(-r^2) t_0 / \tilde{Re}$. The other component of the mean flow, \bar{v}_{11} , remains free at this order and will be determined only at next order.

3.3. Order ϵ^2

At order ϵ^2 , (3.11)–(3.13) become

$$\frac{\partial \hat{\mathbf{u}}_2}{\partial t_0} + \tilde{\mathcal{L}}(\hat{\mathbf{u}}_2) = -\tilde{\mathcal{N}}(\bar{v}_{11}\mathbf{e}_\theta, \hat{\mathbf{u}}_1) - \tilde{\mathcal{N}}(\hat{\mathbf{u}}_1, \bar{v}_{11}\mathbf{e}_\theta) - \tilde{\mathcal{N}}(\hat{\mathbf{u}}_1, \hat{\mathbf{u}}_1) + \overline{\tilde{\mathcal{N}}(\hat{\mathbf{u}}_1, \hat{\mathbf{u}}_1)} + \tilde{\sigma}\hat{\mathbf{u}}_1 - \frac{\partial \hat{\mathbf{u}}_1}{\partial t_1}, \tag{3.25}$$

$$\tilde{\nabla} \cdot \hat{\mathbf{u}}_2 = 0, \tag{3.26}$$

$$\frac{\partial \bar{v}_{11}}{\partial t_1} = \frac{1}{\overline{Re}} \tilde{D}^2 \bar{v}_{11} - \overline{\tilde{\mathcal{N}}(\hat{\mathbf{u}}_1, \hat{\mathbf{u}}_1)} \cdot \mathbf{e}_\theta. \tag{3.27}$$

It should be pointed out that only the mean-flow component $\bar{v}_{11}\mathbf{e}_\theta$ appears in (3.25) because \bar{v}_{10} varies over r , i.e. more slowly than \bar{v}_{11} , since it originates from the viscous diffusion of v_0 .

Using (3.22), (3.27) can be rewritten as

$$\frac{\partial \bar{v}_{11}}{\partial t_1} = |A|^2 f_{11} + \frac{1}{\overline{Re}} \tilde{D}^2 \bar{v}_{11}, \tag{3.28}$$

where

$$f_{11} = -\left(\tilde{\mathcal{N}}^{(-1)}(\tilde{\mathbf{u}}_1, \tilde{\mathbf{u}}_1^*) + \tilde{\mathcal{N}}^{(1)}(\tilde{\mathbf{u}}_1^*, \tilde{\mathbf{u}}_1)\right) \cdot \mathbf{e}_\theta, \tag{3.29}$$

with $\tilde{\mathcal{N}}^{(n)}$ corresponding to $\tilde{\mathcal{N}}$ with $\partial/\partial z$ replaced by ink . The star denotes the complex conjugate.

The nonlinear terms in the right-hand side of (3.25) comprise first and second harmonics. Hence the solution $\hat{\mathbf{u}}_2$ is sought in the form

$$\hat{\mathbf{u}}_2 = \tilde{\mathbf{u}}_{21}(\tilde{r}, t_1) \exp(ikz) + \tilde{\mathbf{u}}_{22}(\tilde{r}, t_1) \exp(2ikz) + c.c., \tag{3.30}$$

giving for each component

$$\tilde{\mathcal{L}}^{(1)}(\tilde{\mathbf{u}}_{21}) = \tilde{\sigma}A\tilde{\mathbf{u}}_1 - \frac{\partial A}{\partial t_1} \tilde{\mathbf{u}}_1 - A\left(\tilde{\mathcal{N}}^{(1)}(\bar{v}_{11}\mathbf{e}_\theta, \tilde{\mathbf{u}}_1) + \tilde{\mathcal{N}}^{(0)}(\tilde{\mathbf{u}}_1, \bar{v}_{11}\mathbf{e}_\theta)\right), \tag{3.31}$$

$$\tilde{\mathcal{L}}^{(2)}(\tilde{\mathbf{u}}_{22}) = -A^2 \tilde{\mathcal{N}}^{(1)}(\tilde{\mathbf{u}}_1, \tilde{\mathbf{u}}_1), \tag{3.32}$$

where $\tilde{\mathcal{L}}^{(n)}$ corresponds to $\tilde{\mathcal{L}}$ with $\partial/\partial z$ replaced by ink . The compatibility condition to find a solution of (3.31) gives (Manneville 1990; Sipp & Lebedev 2007; Meliga *et al.* 2009)

$$\frac{\partial A}{\partial t_1} = \tilde{\sigma}A - \tilde{B}A, \tag{3.33}$$

where

$$\tilde{B}(t_1) = \frac{\left\langle \tilde{\mathbf{u}}_1^\dagger, \tilde{\mathcal{N}}^{(1)}(\bar{v}_{11}\mathbf{e}_\theta, \tilde{\mathbf{u}}_1) + \tilde{\mathcal{N}}^{(0)}(\tilde{\mathbf{u}}_1, \bar{v}_{11}\mathbf{e}_\theta) \right\rangle}{\left\langle \tilde{\mathbf{u}}_1^\dagger, \tilde{\mathbf{u}}_1 \right\rangle}, \tag{3.34}$$

where $\tilde{\mathbf{u}}_1^\dagger$ is the solution of the adjoint operator $\tilde{\mathcal{L}}^{(1)\dagger}$ defined by

$$\langle \mathbf{u}^\dagger, \tilde{\mathcal{L}}^{(1)}(\mathbf{u}) \rangle = \langle \mathbf{u}, \tilde{\mathcal{L}}^{(1)\dagger}(\mathbf{u}^\dagger) \rangle^*, \tag{3.35}$$

where the scalar product is given by

$$\langle \mathbf{u}^\dagger, \mathbf{u} \rangle = \int_0^\infty (u^\dagger u^* + v^\dagger v^* + w^\dagger w^*) r \, dr. \tag{3.36}$$

The adjoint operator reads $\tilde{\mathcal{L}}^\dagger = \mathcal{L}^\dagger - \epsilon \tilde{\sigma}$, where

$$\mathcal{L}^\dagger(\hat{\mathbf{u}}^\dagger) = (\zeta_0 + 2Ro^{-1})\hat{v}^\dagger \mathbf{e}_r - 2(\Omega_0 + Ro^{-1})\hat{u}^\dagger \mathbf{e}_\theta + \rho^{-1} \nabla \hat{p}^\dagger - Re^{-1} \nabla^2 \hat{\mathbf{u}}^\dagger, \tag{3.37}$$

with $\nabla \cdot \hat{\mathbf{u}}^\dagger = 0$ and the same boundary conditions as for the direct problem.

The amplitude equation (3.33) shows that the leading nonlinear effect comes from the first-order mean-flow correction \bar{v}_{11} through B , whereas a nonlinear term due to harmonics would be obtained only at the next order in ϵ from the interaction between $\tilde{\mathbf{u}}_{22}$ and $\hat{\mathbf{u}}_1$. In contrast to the Stuart–Landau equation, the nonlinear effects due to the mean flow and harmonics operate here at different orders because the mean-flow correction \bar{v}_{11} is of order $O(\epsilon)$, like the leading-order perturbation $\hat{\mathbf{u}}_1$ (see (3.15)–(3.17)). Such scaling comes from the fact that the mean-flow correction \bar{v}_{11} is neutral at leading order due to the assumption of a large Reynolds number. The existence of such a neutral mode is related to the fact that the growth rate nearly vanishes for $k = 0$ (figure 1a). In fact, a close-up would show that the growth rate is slightly negative for $k = 0$. In the usual derivation of the Stuart–Landau equation, viscous effects are not considered small so that the Reynolds stresses in the mean flow equation are equilibrated at leading order by viscous effects. This implies that the mean-flow correction is then not neutral and is of order $O(\epsilon^2)$, i.e. one order smaller than the perturbation. This will be discussed further in the next subsection.

In summary, the evolution of the amplitude A can be determined from (3.33) together with (3.28) and (3.34). The mean flow also evolves because of the viscous diffusion of the initial flow according to (3.20). However, this evolution does not affect the evolution of A at leading order.

3.4. Final amplitude equations

In practice, (3.20), (3.28), (3.33) and (3.34) can now be rescaled and expressed in terms of the time t and the original operators \mathcal{N} and D^2 . For simplicity, (3.20) and (3.28) can also be merged into a single equation, giving the system

$$\frac{\partial \bar{v}_1}{\partial t} = |A|^2 f_1 + \frac{1}{Re} D^2(\bar{v}_1 + v_0), \tag{3.38}$$

$$\frac{\partial A}{\partial t} = \sigma A - BA, \tag{3.39}$$

where

$$f_1 = - \left(\mathcal{N}^{(-1)}(\tilde{\mathbf{u}}_1, \tilde{\mathbf{u}}_1^*) + \mathcal{N}^{(1)}(\tilde{\mathbf{u}}_1^*, \tilde{\mathbf{u}}_1) \right) \cdot \mathbf{e}_\theta, \tag{3.40}$$

$$B = \frac{\left\langle \tilde{\mathbf{u}}_1^\dagger, \mathcal{N}^{(1)}(\bar{v}_1 \mathbf{e}_\theta, \tilde{\mathbf{u}}_1) + \mathcal{N}^{(0)}(\tilde{\mathbf{u}}_1, \bar{v}_1 \mathbf{e}_\theta) \right\rangle}{\left\langle \tilde{\mathbf{u}}_1^\dagger, \tilde{\mathbf{u}}_1 \right\rangle}. \tag{3.41}$$

We emphasize that almost the same equations as (3.38)–(3.39) would have been obtained if the fact that the perturbation varies rapidly over the radial coordinate had not been taken into account. The only difference is that the viscous diffusion of \bar{v}_1 would not

be present in (3.38). When this term is neglected, the problem can be reduced further to only two coupled amplitude equations by deriving B with respect to t :

$$\frac{\partial B}{\partial t} = \mu_0 |A|^2 + \frac{\mu}{Re}, \tag{3.42}$$

$$\frac{\partial A}{\partial t} = \sigma A - BA, \tag{3.43}$$

where

$$\mu_0 = \frac{\langle \tilde{\mathbf{u}}_1^\dagger, \mathcal{N}^{(1)}(f_1 \mathbf{e}_\theta, \tilde{\mathbf{u}}_1) + \mathcal{N}^{(0)}(\tilde{\mathbf{u}}_1, f_1 \mathbf{e}_\theta) \rangle}{\langle \tilde{\mathbf{u}}_1^\dagger, \tilde{\mathbf{u}}_1 \rangle}, \tag{3.44}$$

$$\mu = \frac{\langle \tilde{\mathbf{u}}_1^\dagger, \mathcal{N}^{(1)}(D^2 v_0 \mathbf{e}_\theta, \tilde{\mathbf{u}}_1) + \mathcal{N}^{(0)}(\tilde{\mathbf{u}}_1, D^2 v_0 \mathbf{e}_\theta) \rangle}{\langle \tilde{\mathbf{u}}_1^\dagger, \tilde{\mathbf{u}}_1 \rangle}. \tag{3.45}$$

By combining (3.42) and (3.38) without the viscous diffusion of \bar{v}_1 , one can eliminate A and then integrate (3.38) to obtain explicitly the mean-flow correction

$$\bar{v}_1 = \frac{B}{\mu_0} f_1 + \frac{t}{Re} \left(D^2 v_0 - \frac{\mu}{\mu_0} f_1 \right). \tag{3.46}$$

The amplitude equations (3.42)–(3.43) involve an amplitude B in addition to A , like the AB equations for non-dissipative instabilities (Pedlosky 1970; Gibbon & McGuinness 1981) or like the Ginzburg–Landau equation coupled to a mean field in dissipative systems (Siggia & Zippelius 1981; Couillet & Fauve 1985; Renardy & Renardy 1993; Barthelet & Charru 1998; Charru 2011). In the first case, the amplitude B is also a measure of the mean-flow correction resulting from nonlinear effects as in (3.42)–(3.43), but the equations are second order in time and reversible. In the second case, the equations are first order in time as in (3.42)–(3.43), but the amplitude B originates from Galilean invariance and is measuring a slowly modulated mean drift in the direction along which the pattern is periodic. Both cases are therefore different from (3.42)–(3.43), and to our knowledge, these equations, although simple, do not seem to have been derived before.

The particular form of (3.38)–(3.39), or the simplified (3.42)–(3.43), is closely related to the fact that the viscous dissipation of the mean flow, which is by essence due to only horizontal shear, is weak since Re is large. In contrast, the viscous dissipation of the three-dimensional perturbation, which is mostly due to vertical shear, is of order unity thanks to the assumption $k^2/Re = O(1)$ (see § 3.1). For this reason, we have at the same time a three-dimensional perturbation with a small growth rate and a mean-flow correction that is also nearly neutral. This differs, for example, from the primary instability of the Taylor–Couette flow (Davey 1962), where the viscous dissipation of the mean-flow correction is not weak when the perturbation is marginally unstable because the axial wavenumber k and the Reynolds number are considered of order unity. As mentioned already in § 3.3, this is equivalent to the case where the term $\partial \bar{v}_1 / \partial t$ would be negligible compared to the viscous term in (3.38). Then an approximation of \bar{v}_1 could be obtained directly by equating the right-hand side of (3.38) to zero. In other words, the mean-flow correction would be slaved to the three-dimensional perturbation (Manneville 1990). The amplitude B would then be linearly related to $|A|^2$, and (3.39) would become a classical

Re	k	σ	μ_0	μ
500	4.68	0.1436	17.23	2.10
2000	2	0.1216	2.45	1.34
2000	8.6	0.2240	74.74	2.51
2000	23	0.0386	634.34	2.87

Table 1. Values of the coefficients of the amplitude equations (3.42)–(3.43) for different wavenumbers and Reynolds numbers, for $Ro = -4$.

Stuart–Landau equation (Stuart 1960). Actually, this is exactly one of the approximations used by Stuart (1958) in his first approach to describe weakly nonlinear saturation of instabilities.

The values of the coefficients μ_0 and μ are given in table 1 for several values of the wavenumber and Reynolds number, for $Ro = -4$. They are always both positive, meaning that B is positive, so that the nonlinear term of (3.43) is stabilizing. The evolution predicted by (3.38)–(3.39) or (3.42)–(3.43) for these parameters will be seen in detail later, in § 6. In Appendix B, an analytical solution of (3.42)–(3.43) is derived when the viscous term of (3.42) is neglected. In table 1, it can also be remarked that μ_0 increases with k approximately like k^2 when $k \gtrsim 4$, in agreement with the scaling (3.6a–d) since the operator \mathcal{N} is applied twice in its definition (see (3.44) and (3.40)).

4. Semi-linear model

The semi-linear model with a single harmonic (denoted SL-1k) proposed by Yim *et al.* (2020) consists simply in assuming $\hat{\mathbf{u}} = \mathbf{u}_1(r, t) \exp(ikz) + c.c.$ in (2.9)–(2.11), and neglecting the nonlinear term $\mathcal{N}(\hat{\mathbf{u}}, \hat{\mathbf{u}}) + \overline{\mathcal{N}(\hat{\mathbf{u}}, \hat{\mathbf{u}})}$ in (2.10) since it involves second harmonics. In other words, the semi-linear equations are

$$\frac{\partial \bar{v}}{\partial t} = \frac{1}{Re} D^2(\bar{v} + v_0) - \mathcal{N}^{(-1)}(\mathbf{u}_1, \mathbf{u}_1^*) \cdot \mathbf{e}_\theta - \mathcal{N}^{(1)}(\mathbf{u}_1^*, \mathbf{u}_1) \cdot \mathbf{e}_\theta, \tag{4.1}$$

$$\frac{\partial \mathbf{u}_1}{\partial t} + \mathcal{L}^{(1)}(\mathbf{u}_1) = -\mathcal{N}^{(1)}(\bar{v} \mathbf{e}_\theta, \mathbf{u}_1) - \mathcal{N}^{(0)}(\mathbf{u}_1, \bar{v} \mathbf{e}_\theta), \tag{4.2}$$

$$\nabla^{(1)} \cdot \mathbf{u}_1 = 0, \tag{4.3}$$

where $\nabla^{(1)}$ is the operator ∇ with $\partial/\partial z$ replaced by ik .

The difference between the weakly nonlinear equations (3.38)–(3.39) and (4.1)–(4.3) is that the radial profile of the perturbation \mathbf{u}_1 is free to evolve and is not constrained to always keep the shape of the most unstable eigenmode. The shortcoming is that the computational cost to integrate (4.2)–(4.3) is higher than for (3.39).

5. Numerical methods

The numerical methods are identical to those in Yim *et al.* (2020) for both DNS and the SL-1k model. Since three-dimensional DNS (Yim *et al.* 2020) have shown that the vortex remains axisymmetric throughout its evolution, only axisymmetric DNS have been conducted herein. These DNS have been performed with the FreeFEM++ software (Hecht 2012) in axisymmetric cylindrical coordinates ($r > 0, z$). The velocity and pressure are

discretized with Taylor–Hood P2 and P1 elements, respectively. The mesh is refined around the vortex, and the mesh size varies from 0.001 to 0.045 with $\sim 32\,000$ degrees of freedom. To avoid the singularity at $r = 0$, (2.1)–(2.2) are multiplied with r^2 . The first-order backward Euler time scheme is used. The axial domain is chosen to fit several or a single axial wavelength with periodic boundary conditions at each end. Solid boundaries would generate Ekman layers that would affect the evolution of the centrifugal instability, as shown by Orlandi & Carnevale (1999). The radial domain is chosen to be $r = [0, r_{max}]$, with $r_{max} = 6$. The boundary conditions at $r = 0$ are $u = v = 0$ since the flow is axisymmetric (Batchelor & Gill 1962). At $r = r_{max}$, all perturbations are enforced to vanish.

The perturbations \mathbf{u}_1 in the SL-1k model and $\hat{\mathbf{u}}$ in the DNS are initialized by the most unstable perturbation for the wavenumber k :

$$\mathbf{u}_1(r, t = 0) = A_0 \tilde{\mathbf{u}}_1(r), \quad \hat{\mathbf{u}}(r, z, t = 0) = A_0 \tilde{\mathbf{u}}_1(r) e^{ikz} + c.c., \quad (5.1a,b)$$

where A_0 is the initial amplitude, and $\tilde{\mathbf{u}}_1$ is the dominant eigenmode computed from a linear stability analysis based on the Chebyshev pseudo-spectral collocation method (Antkowiak & Brancher 2004). The initial mean-flow correction is set to zero: $\bar{v}(r, t = 0) = 0$. Similarly, the weakly nonlinear equations (3.38)–(3.39) and (3.42)–(3.43) are integrated using an explicit Runge–Kutta formula with initial conditions $A(t = 0) = A_0$, with $\bar{v}_1(r, t = 0) = 0$ or $B(t = 0) = 0$.

6. Comparison between the DNS and the weakly nonlinear and semi-linear models

6.1. Validation of the weakly nonlinear analysis for $Re = 500$

Figure 2 shows the time evolution of the azimuthal velocity field in DNS for $Re = 500$, $Ro = -4$ and initialized by the eigenmode of the most amplified wavenumber $k = 4.68$, with amplitude $A_0 = 0.001$. The growth rate for these parameters is relatively small ($\sigma = 0.1436$) and approaches the condition (3.1) assumed to derive the weakly nonlinear model. In addition, the Reynolds number is not too small so that the condition (3.2) is satisfied reasonably as well. For the smaller Reynolds number $Re = 150$ (figure 1a), the growth rate and the Reynolds number are smaller so that the condition $1/\sqrt{Re} \lesssim \sigma$ is not fully satisfied. Conversely, for the higher Reynolds number $Re = 1000$, the growth rate is larger so that the condition $\sigma \ll 1$ is less well satisfied. Hence the Reynolds number $Re = 500$ is a good compromise to test the weakly nonlinear model. As an aside, we note that the conditions $1/\sqrt{Re} \lesssim \sigma \ll 1$ will be satisfied only for higher and higher Reynolds numbers when the Rossby number tends to $Ro_c = -1$ since the maximum growth rate decreases to zero.

Coming back to figure 2, we see that the perturbations grow and redistribute the azimuthal velocity before decaying. This simulation has been performed over ten wavelengths in order to allow the possible emergence of spatial modulation or the growth of harmonics different from the wavenumber of the initial perturbation. As already reported by Yim *et al.* (2020) for other parameters, figure 2 shows clearly that there is no significant growth of wavenumbers other than the one imposed initially. Indeed, the dynamics of the centrifugal instability on a free isolated vortex differs from that on the well-known Taylor–Couette flow (Di Prima & Swinney 1981; Manneville 1990; Charru 2011). In the latter flow, the mean azimuthal flow is continuously forced and maintained by the rotation of the cylinders so that if the flow is unstable for a given wavenumber, then

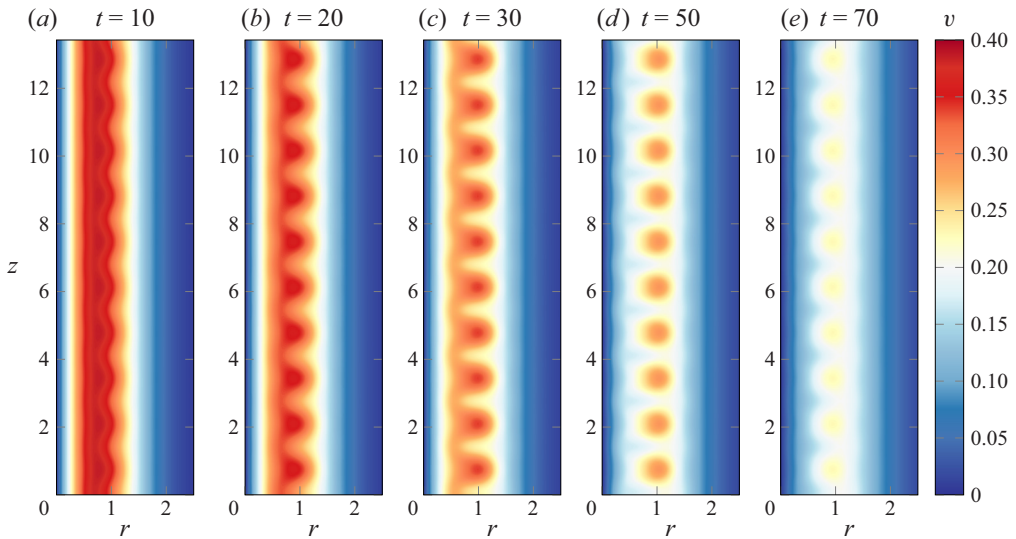


Figure 2. Evolution of the azimuthal velocity field $v(r, z, t)$ in DNS for $Ro = -4$, $k = 4.68$, $A_0 = 0.001$ and $Re = 500$. The axial length corresponds to ten most amplified wavelengths.

spatial modulation and interactions between harmonics have plenty of time to develop. In the case of a free vortex, the centrifugal instability is transient and quite quickly ceases, leaving little time for the development of spatial modulation or for interaction with harmonics. This is the main reason why the weakly nonlinear analysis in § 3 and the semi-linear model SL-1k consider a single axial wavenumber without spatial modulation, in contrast to similar analyses performed for the Taylor–Couette flow.

In order to compare quantitatively this evolution to those predicted by the weakly nonlinear (WNL) and semi-linear (SL-1k) models, three different amplitudes are defined from different velocity components:

$$A = \max(|w|), \quad A_r = \max(|u|), \quad B_{\bar{v}} = \sqrt{\int_0^r (\bar{V} - v_0)^2 r dr}, \quad (6.1a-c)$$

where $\bar{V} - v_0$ is the mean-flow correction, i.e. \bar{v} for the SL-1k model, and \bar{v}_1 for the WNL model. The amplitude A corresponds to that defined in the WNL model. The amplitude A_r is proportional to A in the linear regime and, at any time, in the WNL model. However, A and A_r are no longer linearly related in the nonlinear regime in the DNS and the SL-1k model. The use of the additional amplitude A_r should therefore enable a more comprehensive comparison between the models and the DNS than by considering just A . The third amplitude, $B_{\bar{v}}$, is a measure of the kinetic energy associated with the mean-flow correction. As seen in figure 3 and observed already by Yim *et al.* (2020), the amplitudes A and A_r first grow exponentially, then saturate and decay. In contrast, $B_{\bar{v}}$ grows continuously because of the Reynolds stresses and the viscous diffusion of the mean-flow. From the amplitude equation (3.39), it can be deduced that A is maximum in the WNL model at the time when $B = \sigma$. The evolutions of the amplitudes in the WNL model (solid green lines) are in very good agreement with those in the DNS (dashed red lines) and the SL-1k model (black dash-dotted lines). This validates the asymptotic analysis carried out in § 4. In addition, the dashed green lines show the predictions of the simplified WNL model

Weakly nonlinear versus semi-linear models

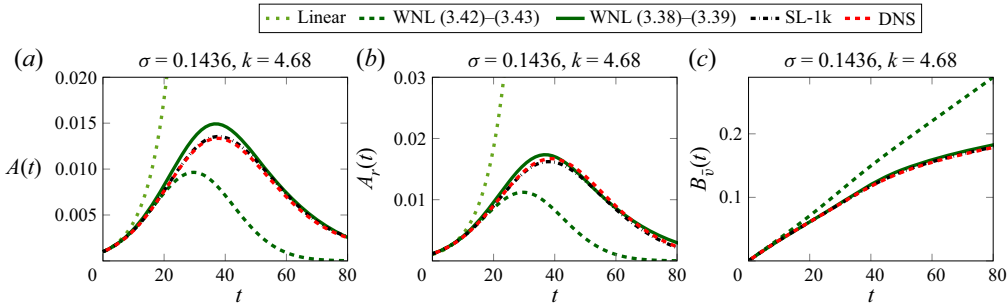


Figure 3. Comparison of the evolution of the amplitudes (a) A , (b) A_r , and (c) $B_{\bar{v}}$, between the different models and the DNS for $k = 4.68$, $A_0 = 0.001$, $Re = 500$ and $Ro = -4$. The different lines correspond to the pure linear growth $A_0 \exp(\sigma t)$ (light green dotted lines), the WNL model (3.38)–(3.39) (solid green lines), the simplified WNL model (3.42)–(3.43) (dashed green lines), the semi-linear model SL-1k (black dash-dotted lines) and DNS (red dashed lines).

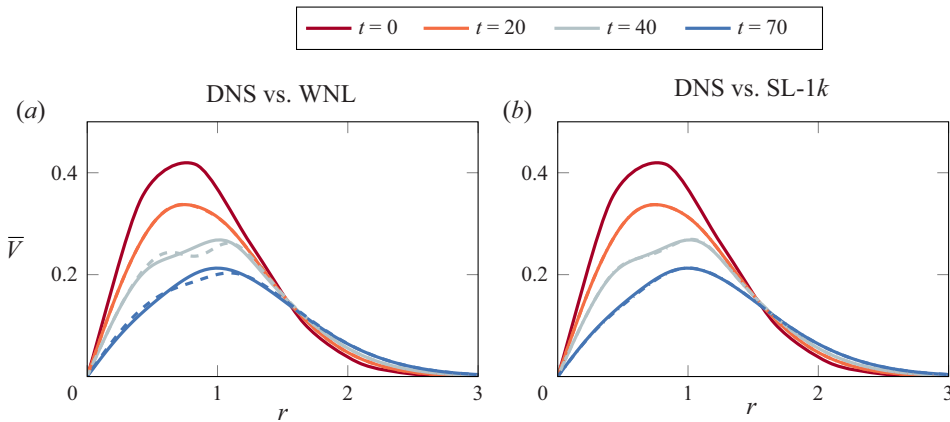


Figure 4. Radial profiles of mean azimuthal velocity \bar{V} at different times for $k = 4.68$, $A_0 = 0.001$, $Re = 500$ and $Ro = -4$. (a) Comparison between the DNS (solid lines) and WNL model (3.38)–(3.39) (dashed lines). (b) Comparison between the DNS (solid lines) and SL-1k model (dash-dotted lines).

(3.42)–(3.43), i.e. when the viscous diffusion of the mean-flow correction is not taken into account. We recall that this term would have been neglected in the asymptotic analysis if the fact that the wavenumber k is large for $Re \gg 1$ had not been taken into account. We see that this simplified WNL model departs from the DNS in contrast to the full WNL model (solid green lines).

Figure 4 further compares the models to the DNS by showing the evolution of the mean azimuthal velocity profiles. The WNL mean flow \bar{V} is in very good agreement with the DNS (figure 4a) as well as that in the SL-1k model (figure 4b). After $t = 40$, a slight difference between the WNL model and the DNS is, however, visible.

6.2. Comparison for $Re = 2000$

Having validated the WNL and SL-1k models for the most amplified wavenumber for $Re = 500$, we now investigate the evolutions of various wavenumbers for a stronger unstable case, $Re = 2000$, still for the same Rossby number $Ro = -4$. Figures 5 and 6 show the time evolution of the azimuthal velocity field in DNS for two different axial wavenumbers:

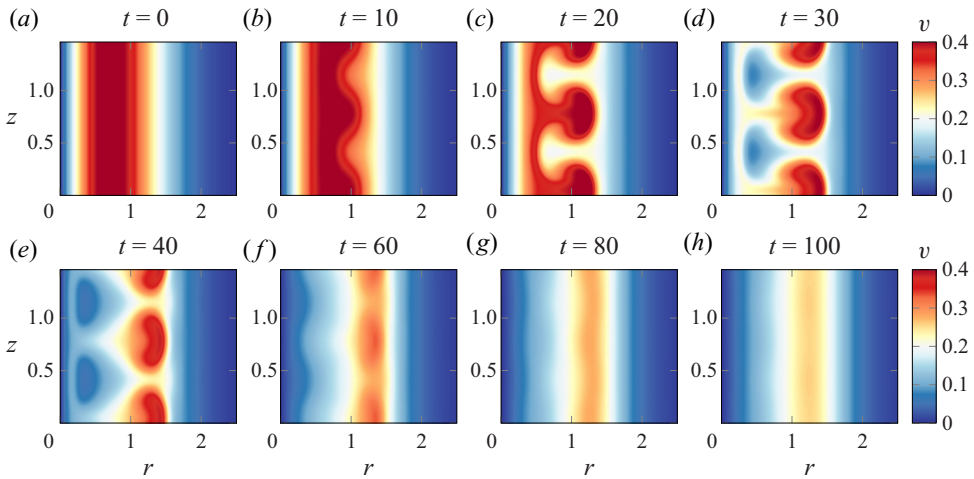


Figure 5. Evolution of the azimuthal velocity field $v(r, z, t)$ in DNS for $Ro = -4$, $k = 8.6$, $A_0 = 0.001$ and $Re = 2000$. Two wavelengths are displayed, although the DNS has actually been performed over only one wavelength.

$k = 8.6$ and $k = 2$. The first value corresponds to the most amplified wavenumber for $Re = 2000$ (figure 1). For these simulations, an axial domain corresponding to a single wavelength has been chosen since Yim *et al.* (2020) and figure 2 showed the absence of significant spatial modulation during the evolution of the centrifugal instability. For both wavenumbers, mushroom-shaped perturbations grow and redistribute the azimuthal velocity before decaying. As expected, this occurs more slowly for $k = 2$ (figure 6) than for $k = 8.6$ (figure 5). In addition, for $k = 2$, the mushrooms deform into chevrons at $t = 60$, indicating the significant growth of higher axial harmonics.

Figure 7 shows the evolution of the amplitudes A , A_r and $B_{\bar{v}}$ for the two axial wavenumbers $k = 8.6$, $k = 2$, and also for $k = 23$. The latter wavenumber is close to the viscous cut-off for $Re = 2000$ and has a small growth rate $\sigma = 0.0386$ (figure 1a). The time evolution of the azimuthal velocity field in these DNS exhibits only weak vertical modulations (at most, as for $t = 20$ in figure 6) and is therefore not shown. The purpose of this simulation is to test again the WNL analysis. Actually, it is much easier to fulfil the assumptions (3.1) and (3.2) near the viscous wavenumber cut-off for large Reynolds number. Indeed, with the Reynolds number fixed to a large value, the particular wavenumber studied can be chosen simply so that its growth rate satisfies $1/\sqrt{Re} \lesssim \sigma \ll 1$.

As can be seen in figures 7(a–c), the evolutions of the amplitudes in the WNL model (solid green lines) are in excellent agreement with those in the DNS (dashed red lines) and the SL-1k model (black dash-dotted lines). Hence the asymptotic analysis carried out in § 4 is also valid close to the viscous cut-off wavenumber for Re far from Re_c . In addition, the dashed green lines show that the predictions of the simplified WNL model (3.42)–(3.43) depart slightly from the DNS in contrast to the full WNL model (solid green lines). Note that DNS with axial size corresponding to several wavelengths for this wavenumber would certainly exhibit the growth of lower wavenumbers since they are more unstable.

For the most amplified wavenumber, $k = 8.6$ (figures 7d–f), there exist more significant differences between the WNL and SL-1k models and the DNS. The WNL model (3.38)–(3.39) predicts that the mean flow amplitude grows and then saturates, in good qualitative agreement with the DNS, but it underestimates the maximum value of $B_{\bar{v}}$

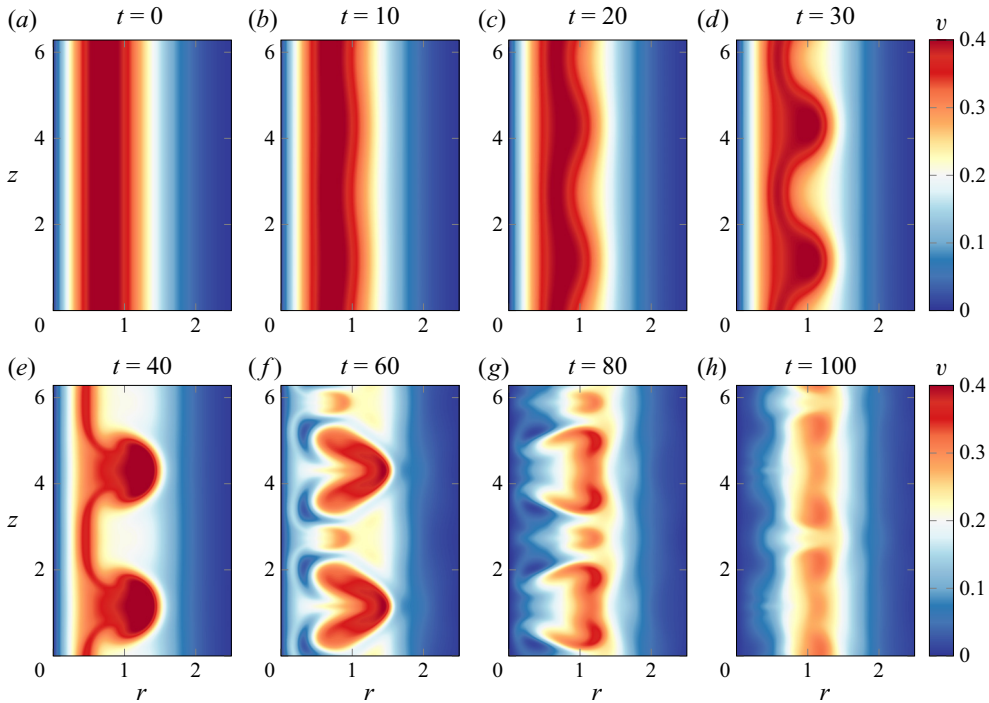


Figure 6. Similar to figure 5, but for $k = 2$.

(figure 7f) and the peaks of the amplitudes A and A_r (figures 7d,e). Such a departure is not surprising since the assumption of a small growth rate used in the asymptotic analysis is no longer satisfied for $k = 8.6$. In contrast, the SL-1k model is in better quantitative agreement with the DNS in terms of the three amplitudes, although some differences are also visible after $t = 20$. The greater ability of the SL-1k model comes from the fact that the spatial structure of the perturbation is not frozen, unlike in the WNL model.

Surprisingly, we can notice that A and A_r are maximum around $t = 20$ for both $k = 8.6$ and $k = 23$, even though the growth rate varies by almost a factor 6 (figure 7). Since A is maximum when $\sigma = B$ in the WNL model, it can be deduced that the corresponding time $t = t_m$ depends not only on the growth rate but also on the speed at which B grows. The analytical solution derived in Appendix B when the viscous decay of the mean flow is neglected shows that the time t_m depends on only σ and $\mu_0 A_0^2$. When $A_0 = 0.001$ as in figure 7, we have approximately $\sigma^2 \gg \mu_0 A_0^2$, so that $t_m \simeq \ln(4\sigma^2/(\mu_0 A_0^2))/(2\sigma)$. The variations of the growth rate σ and the parameter $4\sigma^2/(\mu_0 A_0^2)$ tend to compensate when k is varied from $k = 8.6$ to $k = 23$ (table 1) so that t_m varies very little.

For $k = 2$ (figures 7g–i), the amplitude A of the WNL model predicts surprisingly well the first peak of the DNS. The mean-flow amplitude $B_{\bar{v}}$ is also reasonably well predicted by the WNL model (3.38)–(3.39), but the peak of A_r is underestimated. For this value of k , we see that the predictions of the SL-1k model are close to those of the WNL model, and not particularly better. In addition, we can notice the presence of several peaks in the DNS for both A and A_r . In Appendix A, they are shown to originate from the growth of higher harmonics, whereas by essence, the SL-1k and WNL models take into account a single harmonic.

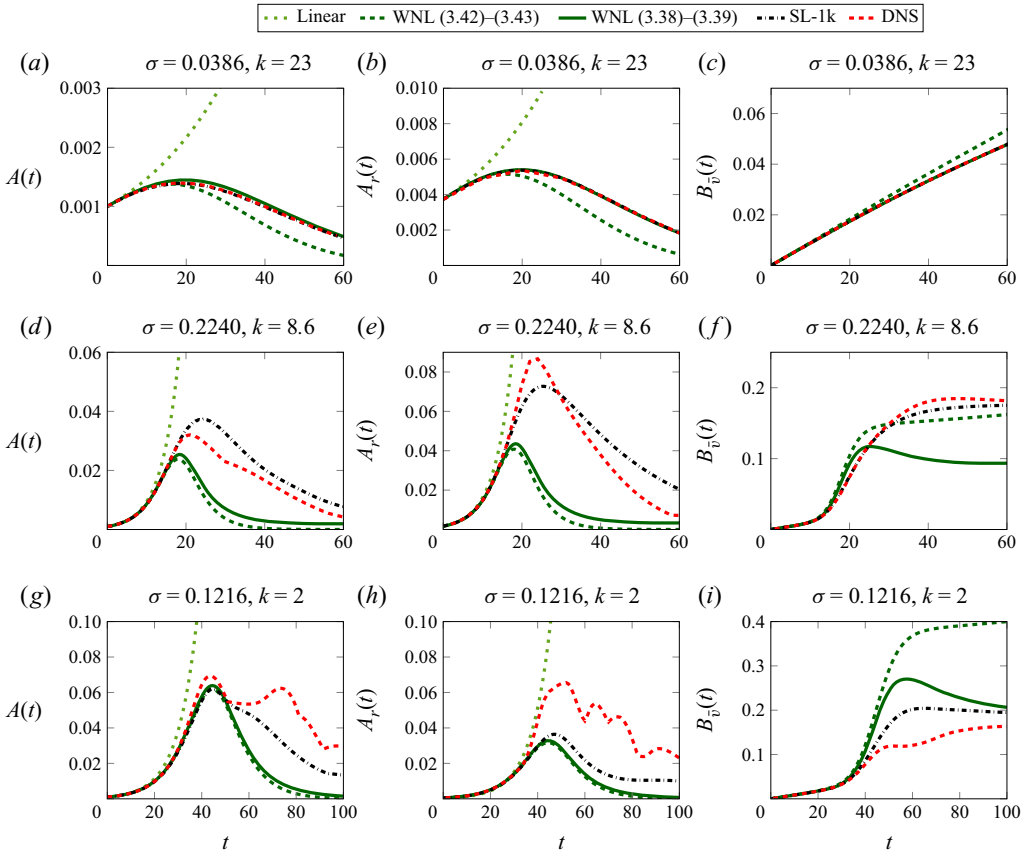


Figure 7. Comparison of the evolution of the amplitudes (a,d,g) A , (b,e,h) A_r , and (c,f,i) $B_{\bar{v}}$, between the different models and the DNS for different axial wavenumbers: (a–c) $k = 23$, (d–f), $k = 8.6$, (g–i) $k = 2$, for $A_0 = 0.001$, $Re = 2000$ and $Ro = -4$. The different lines correspond to the pure linear growth $A_0 \exp(\sigma t)$ (light green dotted lines), the WNL model (3.38)–(3.39) (solid green lines), the simplified WNL model (3.42)–(3.43) (dashed green lines), the semi-linear model SL-1k (black dash-dotted lines) and DNS (red dashed lines).

Finally, it can be remarked that the amplitudes A and A_r in the simplified WNL model (3.42)–(3.43) are very close to the complete WNL model (3.38)–(3.39) for all three wavenumbers for $Re = 2000$ (figure 7). In contrast, there exist differences between the two models regarding $B_{\bar{v}}$ for $k = 8.6$ and $k = 2$, with, paradoxically, a better agreement of the simplified model with the DNS for $k = 8.6$. However, we do not have any particular explanation for this, and in any case, we will see below that even if $B_{\bar{v}}$ is close in the DNS and the WNL model, the profiles of the mean flow \bar{V} differ strongly.

Figure 8 further compares the models to the DNS by showing the evolution of the mean azimuthal velocity profiles for $Re = 2000$ for the three wavenumbers. For $k = 23$, the WNL mean flow is in very good agreement with the DNS (figure 8a) as well as the SL-1k model (figure 8b). In contrast, we can see in figures 8(c,e) that the mean-flow profiles predicted by the WNL model differ largely from the DNS for both $k = 8.6$ and $k = 2$. The predictions of the SL-1k model are in much better agreement with the DNS (figures 8d,f). This is due to the fact that the spatial structure of the growing unstable perturbation is free to evolve in the SL-1k model and can adapt to the change of the mean flow, whereas in the WNL model, the perturbation at leading order always keeps the spatial structure of the

Weakly nonlinear versus semi-linear models

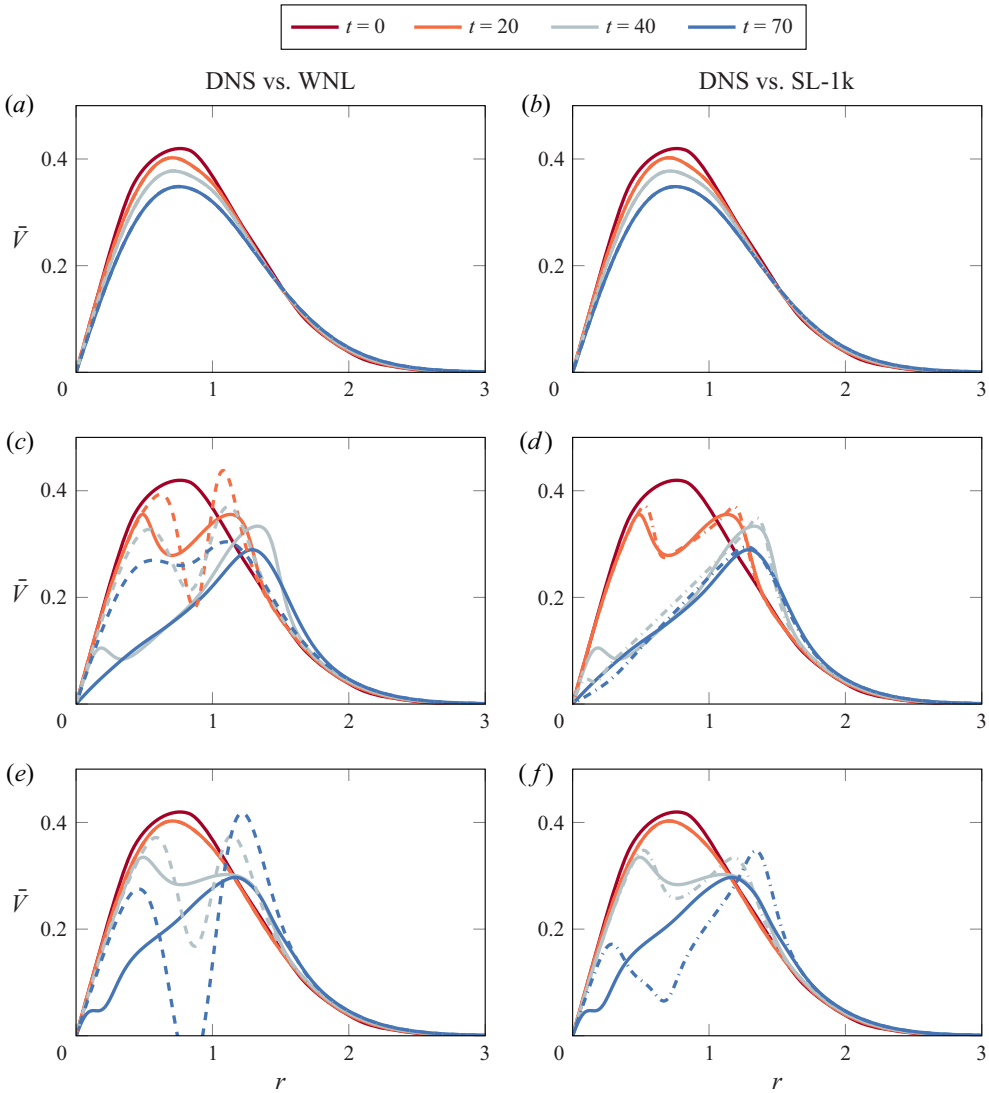


Figure 8. Radial profiles of mean azimuthal velocity \bar{V} at different times for different wavenumbers: (a,b) $k = 23$, (c,d) $k = 8.6$, and (e,f) $k = 2$, for $Re = 2000$ and $Ro = -4$. (a,c,e) Comparison between the DNS (solid lines) and WNL model (3.38)–(3.39) (dashed lines). (b,d,f) Comparison between the DNS (solid lines) and SL-1k model (dash-dotted lines).

eigenmode of the initial mean flow. As an illustration, figure 9 shows that the radial profiles of the vertical velocity in the WNL and SL-1k models, i.e. $A\tilde{w}_1$ and w_1 , respectively, remain always very close for $k = 23$ but differ for $k = 8.6$ for $t \geq 20$.

The evolutions of the three amplitudes A , A_r , $B_{\bar{v}}$ of the WNL model for $Re = 2000$ are summarized in figure 10(a–c) for various wavenumbers. The time at which the amplitudes A and A_r reach their maxima is minimum around the most amplified wavenumber $k_{max} = 8.6$. Interestingly, the overall value of the maximum amplitude is reached not when $k = k_{max}$ but for a lower wavenumber that depends on the amplitude considered. For A , the maximum value is reached for $k = 2$, while for A_r , it is around $k = 5$. Such a

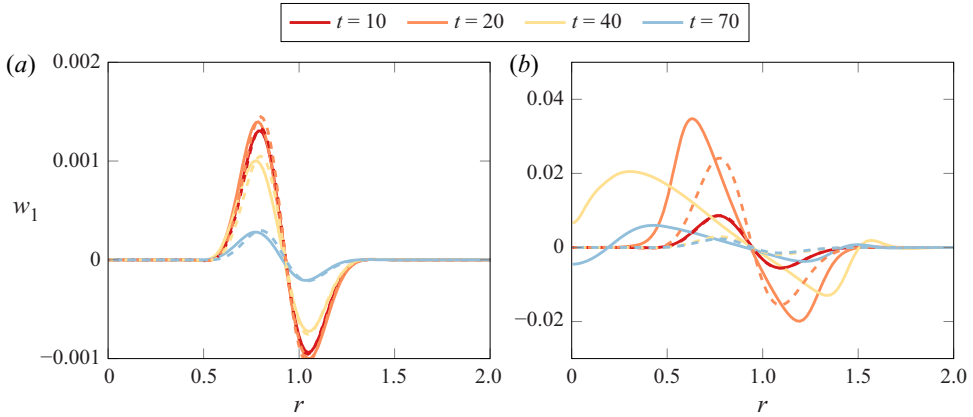


Figure 9. Comparison between the vertical velocity profile in the WNL model, $A\tilde{w}_1$ (dashed line), and in the SL-1k model, w_1 (solid line) for (a) $k = 23$, and (b) $k = 8.6$, for $Re = 2000$ and $Ro = -4$.

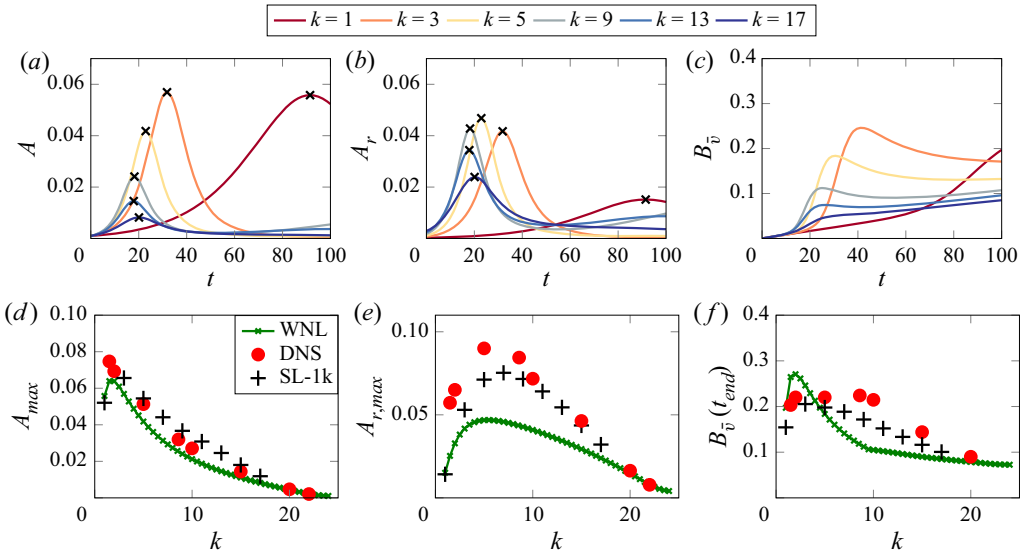


Figure 10. Evolutions of the amplitudes (a) A , (b) A_r and (c) $B_{\bar{v}}$ in the WNL model (3.38)–(3.39) as functions of time for different wavenumbers k , for $A_0 = 0.001$, $Re = 2000$ and $Ro = -4$. Maxima of the amplitudes (d) A , (e) A_r and (f) $B_{\bar{v}}(t_{end})$ as functions of k , with $t_{end} = 100$. The symbols are green crosses for the WNL model (3.38)–(3.39), red circles for the DNS, and plus symbols for the SL-1k model.

difference is possible because the ratio $\max(\tilde{w}_1)/\max(\tilde{u}_1) = A_{max}/A_{r,max}$ is different for each eigenmode and thus for each value of k .

The maximum values of the amplitudes for each k are compared to the DNS and the SL-1k model in figures 10(d–f). We can see that there is a good agreement with the DNS and the SL-1k model regarding A_{max} (figure 10d). In the DNS, the amplitude A_{max} does not decrease with k when $k \leq 2$, in contrast to the WNL and SL-1k models. For k of order unity, the evolution of A exhibits several peaks in the DNS, as seen in figure 7(a); and for $k \lesssim 2$, the overall maximum is reached by the second peak. Since this second peak is due

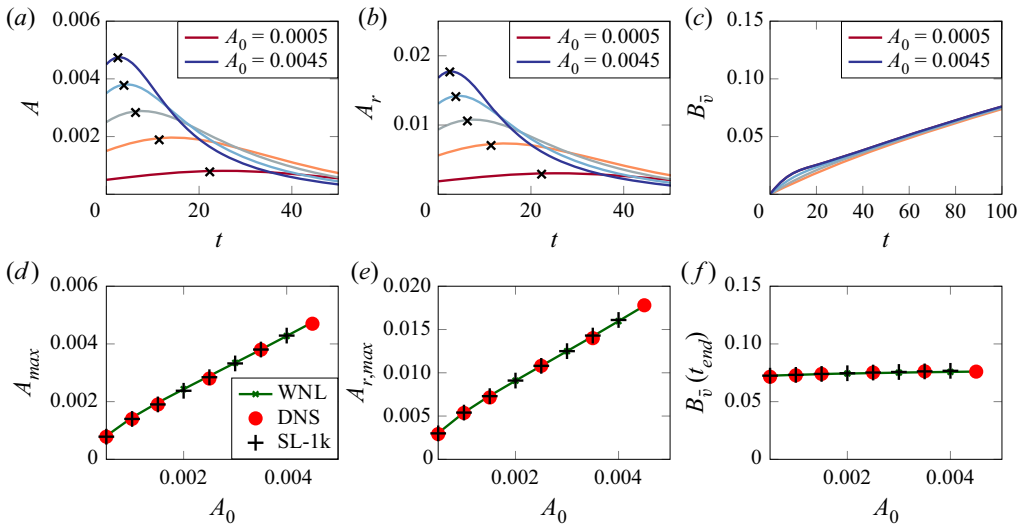


Figure 11. Evolutions of the amplitudes (a) A , (b) A_r and (c) $B_{\bar{v}}$ in the WNL model (3.38)–(3.39) as functions of time for different initial amplitudes $A_0 = [0.0005 : 0.001 : 0.0045]$ for $k = 23$, $Re = 2000$ and $Ro = -4$. Maxima of the amplitudes (d) A , (e) A_r and (f) $B_{\bar{v}}(t_{end})$ as functions of A_0 , with $t_{end} = 100$. The symbols are green crosses for the WNL model (3.38)–(3.39), red circles for the DNS, and plus symbols for the SL-1k model.

to the growth of higher harmonics (see Appendix A), it cannot be captured by the WNL and SL-1k models, which take into account a single harmonic.

The agreement between the WNL model and the DNS is not very good regarding A_r when $k \lesssim 15$ (figure 10e). Nevertheless, the maximum amplitude $A_{r,max}$ is reached around $k \sim 3-5$ for both the DNS and the WNL and SL-1k models. The amplitude A_r of the SL-1k model agrees much better with the DNS. Finally, figure 10(f) shows that the amplitude of the mean flow at $t = t_{end} = 100$ is almost independent of k for $1 \leq k \leq 10$, meaning that the global effect of the instability on the mean vortex profile is the same even if A_{max} and $A_{r,max}$ vary with k . Again, we can see that the SL-1k model is in better agreement with the DNS than the WNL model for $k \lesssim 10$. Note that the amplitude $B_{\bar{v}}$ is considered at the particular time $t_{end} = 100$ because in addition to the rapid evolution towards saturation due to the centrifugal instability, it slowly evolves due to the viscous diffusion of the mean flow. At the time $t_{end} = 100$, the instability has grown and just ceased for most wavenumbers. Hence it measures mostly the effect of the centrifugal instability and not the diffusion of the mean flow.

Figure 11 displays similar comparisons when the wavenumber is fixed at $k = 23$, but the initial amplitude A_0 varies. As can be seen, the maximum amplitudes A_{max} and $A_{r,max}$ increase with A_0 . However, $B_{\bar{v}}(t_{end})$ is almost independent of A_0 . We can see that the agreement is very good for this case, as expected, since the perturbations are marginally unstable for $k = 23$ as assumed in the WNL analysis.

7. Conclusions

We have developed a weakly nonlinear (WNL) analysis of the centrifugal instability for a vortex with Gaussian angular velocity in a rotating fluid for large Reynolds number. The Rossby number has been considered far from the threshold $Ro_c = -1$, but the Reynolds number has been assumed to be close to the critical value for a given wavenumber so that

the perturbations are marginally unstable. This leads to an equation for the amplitude A of the disturbances whose leading nonlinear term comes from the stabilizing correction of the mean flow. In turn, the mean flow evolves under the Reynolds stresses of the perturbations, which are quadratic in amplitude (i.e. $|A|^2$), and also under its own viscous dissipation. Since the Reynolds number is assumed to be large, the latter viscous effects for the mean-flow correction are weak, implying that it is not slaved to the perturbations as usual for other systems, like, for example, the Taylor vortices in the Taylor–Couette flow. This feature is the main reason why the present equations differ from the Stuart–Landau equation (Stuart 1960; Manneville 1990) or from other types of amplitude equations involving a mean field (Gibbon & McGuinness 1981; Couillet & Fauve 1985; Barthelet & Charru 1998). This difference is reflected in the qualitative behaviour of the amplitude A , which does not tend to a constant as in the Stuart–Landau equation for supercritical instabilities, but decays after a certain time. This comes from the fact that the mean flow saturates towards a neutrally stable profile in the DNS. A similar behaviour (growth and subsequent decay of the amplitude A) is observed for dispersive systems, like for the Kelvin–Helmholtz or baroclinic instabilities (Drazin 1970; Pedlosky 1970; Gibbon & McGuinness 1981). However, in the latter cases, the growth and decay of the amplitude A repeats periodically with time since the amplitude equations are second order in time and reversible. Here, the growth of A is observed only once as in the DNS because the system is dissipative and the equations are first order in time.

Quantitative comparisons between the WNL model, DNS and the empirical semi-linear model SL-1k (Yim *et al.* 2020) have been presented. In order to quantify precisely the evolution of the perturbations, two amplitudes have been defined in addition to the amplitude A that is defined as the maximum axial velocity in the WNL analysis. The amplitude A_r measures the maximum radial velocity, while $B_{\bar{v}}$ quantifies the mean-flow correction. The amplitudes A and A_r are linearly related in the WNL model but not in the nonlinear regime of the SL-1k model and in the DNS. The two models and the DNS agree very well in terms of the three amplitudes and the mean flow profiles for the most amplified wavenumber when the Reynolds number is moderate, i.e. when it is both not too large and not too far from the critical value. Indeed, the condition of validity of the WNL analysis is not only that the growth rate should be small, but it should also be of the same order or larger than $1/\sqrt{Re}$. Otherwise, the viscous diffusion of the mean flow is too fast compared to the slow growth of the perturbation. The agreement between the WNL model and the DNS is also very good when the axial wavenumber is close to the viscous wavenumber cut-off for arbitrary Reynolds number. However, as for time-periodic instabilities (Mantič-Lugo *et al.* 2014; Meliga 2017), the accuracy of the predictions of the WNL equations for the present spatially periodic instability deteriorates as one significantly departs from the marginal value. In contrast, the predictions of the semi-linear model, although empirical, are more quantitatively robust and accurate. The main difference between the two models is that the spatial structure of the growing unstable mode at leading order is fixed by the unperturbed base flow in the WNL model, while it is free to evolve under the change of the mean flow in the SL-1k model.

Nevertheless, it is worth pointing out that the agreement between the WNL and semi-linear models close to the critical Reynolds number or viscous wavenumber cut-off provides a rigorous justification of the empirical semi-linear model and, in particular, the fact that harmonics can then be neglected legitimately. Indeed, while this approximation is not valid for the primary instabilities of the plane Poiseuille or Taylor–Couette flows near the marginal value of the control parameter (Stuart 1958, 1960; Davey 1962), the present

WNL analysis of the centrifugal instability shows that the effect of higher harmonics is one order of magnitude smaller than the interaction between the mean flow and the fundamental mode.

In the future, it could be interesting to perform a WNL analysis of the centrifugal instability in the inviscid limit for Rossby numbers close to the critical Rossby number $Ro_c = -1$. In this case, the distance $1/Ro - 1/Ro_c$ can be used as a small parameter. The resulting amplitude equations will differ from those derived herein because the instability then arises in the form of a pair of marginally stable/unstable eigenmodes. They should be closer to those derived previously for other inviscid instabilities (Drazin 1970; Pedlosky 1970; Gibbon & McGuinness 1981).

Acknowledgements. We thank P. Manneville for fruitful discussions and the referees for their comments that have greatly improved the paper.

Declaration of interests. The authors report no conflict of interest.

Author ORCIDs.

 Eunok Yim <https://orcid.org/0000-0003-4776-1598>;

 Paul Billant <https://orcid.org/0000-0002-0784-5300>;

 François Gallaire <https://orcid.org/0000-0002-3029-1457>.

Appendix A. Contributions of higher harmonics for low wavenumber in the DNS

In order to understand why several peaks are observed in the evolution of the amplitude A in the DNS when the wavenumber is around unity (figure 7g), we investigate here in more detail DNS performed for $k = 1.5$, $Re = 2000$, $A_0 = 0.001$ and $Ro = -4$. As can be seen from the black line in figure 12, the amplitude A exhibits two peaks, the second being dominant. The decomposition of the contributions of each harmonic to A shows that the second harmonic becomes larger than the first for $60 < t \lesssim 70$, while higher harmonics also grow significantly. Hence the growth of higher harmonics explains the occurrence of several peaks. The deformation of the azimuthal velocity perturbations into chevrons seen in figure 6 is also a signature of the emergence of higher harmonics.

Appendix B. Exact solution of (3.42)–(3.43) when $\mu = 0$

Here, we show that the amplitude equations (3.42)–(3.43) can be integrated analytically when the viscous term of (3.42) is neglected (i.e. $\mu = 0$). We first add together (3.43) multiplied by A^* , and its complex conjugate multiplied by A . By combining the resulting equation with (3.42) and integrating, we obtain

$$|A|^2(t) = \frac{2\sigma}{\mu_0} B(t) - \frac{B(t)^2}{\mu_0} + |A_0|^2, \quad (\text{B1})$$

where it has been imposed that $B(0) = 0$, and assumed that σ and μ_0 are real. Hence (3.42) can be written solely in terms of B :

$$\frac{\partial B}{\partial t} = 2\sigma B - B^2 + \mu_0 |A_0|^2. \quad (\text{B2})$$

The solution can be found in the form

$$B = \mu_0 |A_0|^2 \frac{1 - \exp(-2\alpha t)}{(\sigma + \alpha) \exp(-2\alpha t) - \sigma + \alpha}, \quad (\text{B3})$$

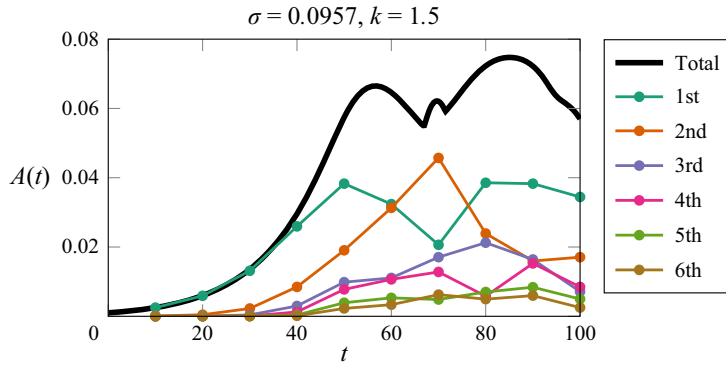


Figure 12. Contributions of the first six harmonics (coloured lines with circle symbols) to the amplitude A (black line) for $k = 1.5$, $Re = 2000$, $A_0 = 0.001$ and $Ro = -4$.

where $\alpha = \sqrt{\sigma^2 + \mu_0 |A_0|^2}$. Then the solution for A can be found from (3.42):

$$A = A_0 \frac{2\alpha \exp(-\alpha t)}{(\sigma + \alpha) \exp(-2\alpha t) - \sigma + \alpha}. \quad (\text{B4})$$

When $\mu_0 > 0$, the solutions (B3)–(B4) show clearly that A vanishes for $t \rightarrow \infty$, while B tends to the constant $\mu_0 |A_0|^2 / (\alpha - \sigma)$. The maximum value of A is $\alpha / \sqrt{\mu_0}$, which is reached for $t = t_m \equiv -\ln((\alpha - \sigma) / (\alpha + \sigma)) / (2\alpha)$. When μ is non-zero and positive, an analytical solution of (3.42)–(3.43) does not seem to exist, but the behaviour of the amplitude A is qualitatively similar, as seen in § 6. A slow linear increase of the amplitude B is mixed with the solution (B3).

REFERENCES

- ANTKOWIAK, A. & BRANCHER, P. 2004 Transient energy growth for the Lamb–Oseen vortex. *Phys. Fluids* **16**, L1–L4.
- BARTHELET, P. & CHARRU, F. 1998 Benjamin–Feir and Eckhaus instabilities with Galilean invariance: the case of interfacial waves in viscous shear flows. *Eur. J. Mech. B/Fluids* **17** (1), 1–18.
- BATCHELOR, G.K. & GILL, A.E. 1962 Analysis of the stability of axisymmetric jets. *J. Fluid Mech.* **14** (4), 529–551.
- BAYLY, B.J. 1988 Three-dimensional centrifugal-type instabilities in inviscid two-dimensional flows. *Phys. Fluids* **31** (1), 56–64.
- BILLANT, P. & GALLAIRE, F. 2005 Generalized Rayleigh criterion for non-axisymmetric centrifugal instabilities. *J. Fluid Mech.* **542**, 365–379.
- CARNEVALE, G.F., KLOOSTERZIEL, R.C., ORLANDI, P. & VAN SOMMEREN, D.D.J.A. 2011 Predicting the aftermath of vortex breakup in rotating flow. *J. Fluid Mech.* **669**, 90–119.
- CHARRU, F. 2011 *Hydrodynamic Instabilities*. Cambridge University Press.
- COULLET, P. & FAUVE, S. 1985 Propagative phase dynamics for systems with Galilean invariance. *Phys. Rev. Lett.* **55** (26), 2857.
- DAVEY, A. 1962 The growth of Taylor vortices in flow between rotating cylinders. *J. Fluid Mech.* **14** (3), 336–368.
- DI PRIMA, R.C. & SWINNEY, H.L. 1981 Instabilities and transition in flow between concentric rotating cylinders. In *Hydrodynamic Instabilities and the Transition to Turbulence* (ed. H.L. Swinney & J.P. Gollub), Topics in Applied Physics, vol. 45, pp. 139–180. Springer.
- DRAZIN, P.G. 1970 Kelvin–Helmholtz instability of finite amplitude. *J. Fluid Mech.* **42** (2), 321–335.
- GALLAIRE, F., BOUJO, E., MANTIC-LUGO, V., ARRATIA, C., THIRIA, B. & MELIGA, P. 2016 Pushing amplitude equations far from threshold: application to the supercritical Hopf bifurcation in the cylinder wake. *Fluid Dyn. Res.* **48** (6), 061401.

- GIBBON, J.D. & MCGUINNESS, M.J. 1981 Amplitude equations at the critical points of unstable dispersive physical systems. *Proc. R. Soc. Lond. A* **377** (1769), 185–219.
- HECHT, F. 2012 New development in FreeFEM++. *J. Numer. Maths* **20** (3–4), 251–265.
- KLOOSTERZIEL, R.C., CARNEVALE, G.F. & ORLANDI, P. 2007 Inertial instability in rotating and stratified fluids: barotropic vortices. *J. Fluid Mech.* **583**, 379–412.
- MANNEVILLE, P. 1990 *Dissipative Structures and Weak Turbulence*. Academic.
- MANTIČ-LUGO, V., ARRATIA, C. & GALLAIRE, F. 2014 Self-consistent mean flow description of the nonlinear saturation of the vortex shedding in the cylinder wake. *Phys. Rev. Lett.* **113**, 084501.
- MELIGA, P. 2017 Harmonics generation and the mechanics of saturation in flow over an open cavity: a second-order self-consistent description. *J. Fluid Mech.* **826**, 503–521.
- MELIGA, P., CHOMAZ, J.-M. & SIPP, D. 2009 Global mode interaction and pattern selection in the wake of a disk: a weakly nonlinear expansion. *J. Fluid Mech.* **633**, 159–189.
- ORLANDI, P. & CARNEVALE, G.F. 1999 Evolution of isolated vortices in a rotating fluid of finite depth. *J. Fluid Mech.* **381**, 239–269.
- PEDLOSKY, J. 1970 Finite-amplitude baroclinic waves. *J. Atmos. Sci.* **27** (1), 15–30.
- RENARDY, M. & RENARDY, Y. 1993 Derivation of amplitude equations and analysis of sideband instabilities in two-layer flows. *Phys. Fluids A* **5** (11), 2738–2762.
- SIGGIA, E.D. & ZIPPELIUS, A. 1981 Pattern selection in Rayleigh–Bénard convection near threshold. *Phys. Rev. Lett.* **47** (12), 835–838.
- SIPP, D. & LEBEDEV, A. 2007 Global stability of base and mean flows: a general approach and its applications to cylinder and open cavity flows. *J. Fluid Mech.* **593**, 333–358.
- SMYTH, W.D. & MCWILLIAMS, J.C. 1998 Instability of an axisymmetric vortex in a stably stratified, rotating environment. *Theor. Comput. Fluid Dyn.* **11** (3–4), 305–322.
- STUART, J.T. 1958 On the non-linear mechanics of hydrodynamic stability. *J. Fluid Mech.* **4** (1), 1–21.
- STUART, J.T. 1960 On the non-linear mechanics of wave disturbances in stable and unstable parallel flows. Part 1. The basic behaviour in plane Poiseuille flow. *J. Fluid Mech.* **9** (3), 353–370.
- WATSON, J. 1960 On the non-linear mechanics of wave disturbances in stable and unstable parallel flows. Part 2. The development of a solution for plane Poiseuille flow and for plane Couette flow. *J. Fluid Mech.* **9** (3), 371–389.
- YIM, E., BILLANT, P. & GALLAIRE, F. 2020 Nonlinear evolution of the centrifugal instability using a semilinear model. *J. Fluid Mech.* **897**, A34.